

# Modification on Flower Defects and Electronic Properties of Epitaxial Graphene by Erbium

Yong Duan, Wenting Xu, Wenxia Kong, Jianxin Wang, Jinzhe Zhang, Zhongqin Yang, and Qun Cai\*

Cite This: *ACS Omega* 2023, 8, 37600–37609

Read Online

ACCESS |



Metrics &amp; More



Article Recommendations



Supporting Information

**ABSTRACT:** Manipulating the topological defects and electronic properties of graphene has been a subject of great interest. In this work, we have investigated the influence of Er predeposition on flower defects and electronic band structures of epitaxial graphene on SiC. It is shown that Er atoms grown on the SiC substrate actually work as an activator to induce flower defect formation with a density of  $1.52 \times 10^{12} \text{ cm}^{-2}$  during the graphitization process when the Er coverage is 1.6 ML, about 5 times as much as that of pristine graphene. First-principles calculations demonstrate that Er greatly decreases the formation energy of the flower defect. We have discussed Er promoting effects on flower defect formation as well as its formation mechanism. Scanning tunneling microscopy (STM) and Raman and X-ray photoelectron spectroscopy (XPS) have been utilized to reveal the Er doping effect and its modification to electronic structures of graphene. N-doping enhancement and band gap opening can be observed by using angle-resolved photoemission spectroscopy (ARPES). With Er coverage increasing from 0 to 1.6 ML, the Dirac point energy decreases from  $-0.34$  to  $-0.37$  eV and the band gap gradually increases from 320 to 360 meV. The opening of the band gap is attributed to the synergistic effect of substitution doping of Er atoms and high-density flower defects.

## INTRODUCTION

Graphene, a two-dimensional carbon-based material with a honeycomb lattice, has attracted great interests in recent years because of its remarkable electronic and mechanical properties and compatibility with silicon-based circuits.<sup>1–4</sup> In particular, the extremely high mobility and considerable controllability of charge carriers by applying a gate voltage have made graphene a promising material for next-generation electronics with properties that may exceed those of conventional semiconductors.<sup>5–7</sup> As the valence and conduction bands are degenerate at the Dirac point, graphene is a zero-gap semiconductor, limiting its further application in the semiconductor industry. Therefore, we need to induce a band gap at the Dirac point, leading to a semiconducting phase and ultimately to induce spin splitting of the Dirac cone for spintronic applications; thus, how to induce a gap is crucial for its application in making devices.<sup>8,9</sup> Among the various methods used to grow graphene, thermal decomposition of SiC substrates at elevated temperatures is one of the most promising routes for mass-scale graphene fabrication, which exhibits great potential for the application of electronics because of its ability to fabricate wafer-size high-quality graphene and convenience for direct processing on the semi-insulating substrate without transfer.<sup>10,11</sup> However, so far, the electronic band gap of epitaxial graphene (EG) on SiC is insufficient to meet the requirement for fabrication of a large-scale integrated circuit. Band gap broadening is still the near-term target for EG application.

In general, a band gap can be induced in EG by the interaction between EG and a certain substrate (such as single-crystal Cu (111)),<sup>12</sup> by the periodic modulation of the graphene lattice (breaking the sublattice symmetry), by the

stacking of multiple graphene layers,<sup>13</sup> or by the structural confinement in graphene nanoribbons.<sup>14</sup> Wang et al. directly observed the global elastic scattering in graphene after inducing various and abundant impurities.<sup>15</sup> Their results proved that impurities can fundamentally modify the graphene band structure and induce a folded Dirac band with a superstructure due to quantum interference below the critical temperature. Alternatively, an attractive route to induce a gap at Dirac points is to intercalate atomic species into the graphene/substrate interfaces. It has been shown that a wide variety of intercalants such as In,<sup>16</sup> Bi,<sup>17</sup> Mn,<sup>18</sup> Si,<sup>19</sup> and Na<sup>20</sup> can penetrate through the graphene and buffer layer at certain annealing temperature and effectively weaken the strong bonding interaction at the buffer layer/substrate interface region. Apart from decoupling effects, the intercalation process can also change the carrier concentration in graphene and even regulate electron (or hole) doping of graphene, resulting in band gap opening. Research has also shown that magnetic atoms on graphene can be used for spintronic applications, which demands further understanding of the growth behaviors of magnetic atom-doped graphene. Rare-earth metals have large bulk magnetic moments, so they are good candidates for such applications.<sup>21</sup> In contrast to the extensive studies on the intercalation of the atoms mentioned above, erbium is a rare-earth metal with a higher chemical reactivity and larger

Received: August 31, 2023

Accepted: September 15, 2023

Published: September 29, 2023



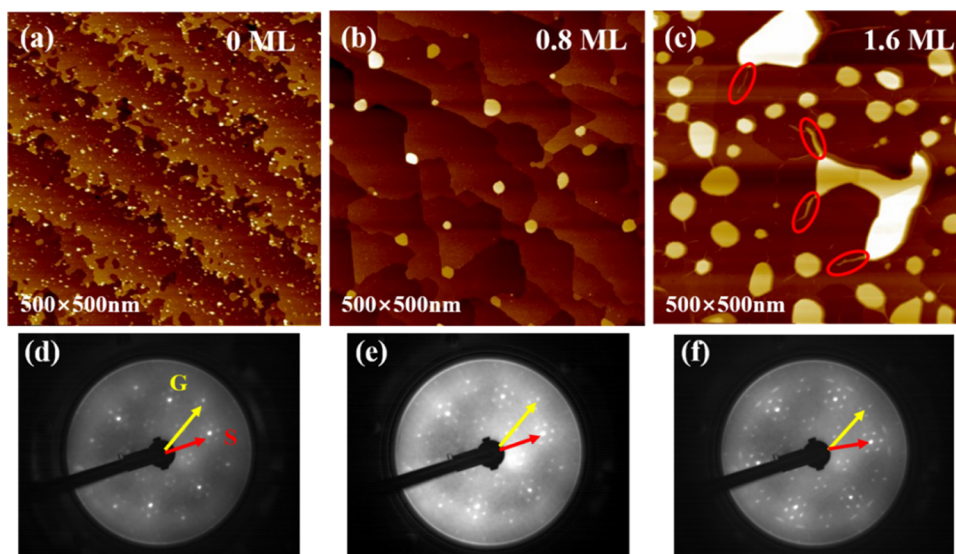


**Figure 1.** (a) Typical STM image of EG/SiC and surface morphology of the EG/SiC sample with (b) 0.8 ML and (c) 1.6 ML Er predeposition. (d–f) LEED patterns of (a–c) samples, respectively. Examples of SiC(S) and graphene(G) spots are marked. Note the surrounding hexagons of “6 × 6” spots. Image parameters: (a) −1.8 V, 1.1 nA; (b) −1.8 V, 1.0 nA; and (c) −2 V, 0.9 nA, LEED incident beam energy: 160 eV.

magnetic moment than those of noble metals,<sup>22</sup> and its effects have not yet been investigated adequately on the electronic properties of EG. It is expected that the Er-doped graphene system will present fascinating physical properties from the viewpoint of energy band modifications and studies.

In this work, a certain amount of Er has been predeposited on the clean SiC substrate surface, and after annealing treatments, we have explored the effects of Er growth with different coverages on the structural defects and electronic properties of EG. Scanning tunneling microscopy (STM) results and theoretical calculations show that Er atoms increase the areal density of flower defects (FDs) by reducing their formation energy significantly. Raman spectroscopy and X-ray photoelectron spectroscopy (XPS) have been utilized to analyze electron doping in graphene induced by Er deposition as well as the interaction of graphene and the SiC substrate. According to the obtained results, we discuss the promoting effect of Er atoms on FD formation in parallel with the FD formation mechanism. In addition, the angle-resolved photoemission spectroscopy (ARPES) results show that the Er growth can open a band gap in EG and that the Er coverage has a modulating effect on the gap, with its width enlarging as the coverage increases.

## 2. EXPERIMENTAL SECTION

**2.1. Sample Preparation.** The experiments were mainly conducted in an ultrahigh-vacuum (UHV) system with a base pressure of  $1.5 \times 10^{-10}$  mbar, equipped with a commercial Omicron room-temperature STM chamber. The data-processing system was Matrix 3.1. The n-type 4H-SiC(0001) substrates were degassed at 950 °C for 30 min and then annealed at about 1100 °C for 26 min via direct current heating to remove oxides and contaminations. Prior to graphene growth, Er was predeposited onto the clean SiC substrate at room temperature for 1–8 min from an electron-beam heated evaporator (evaporation rate of  $\approx 0.2$  ML/min, measured using a quartz-crystal microbalance), and the sample was subsequently postannealed at 600–1300 °C for a few minutes. After each stage of annealing, the sample was cooled

to room temperature and then transferred to an STM chamber for the exploration of its surface morphology.

**2.2. Characterization Methods.** The STM measurements were performed in constant current mode in an Omicron UHV STM system. The STM tips were prepared by electrochemical etching of polycrystalline tungsten wires. All STM images were acquired under the samples biased at −2.4 to 2.0 V and tunneling current at 0.6–1.2 nA. After STM observations, the samples were transferred to a glovebox for remounting, which was under an argon (Ar) atmosphere and connected with a low-energy electron diffraction (LEED) and ARPES system, by using a vacuum suitcase without being exposed to air. The samples were heated for degassing before LEED and ARPES measurements. ARPES measurements were performed on the samples with a Fermi Instruments 21.2 eV helium discharge lamp, using a Scienta DA30 electron analyzer, under a typical vacuum of  $2.5 \times 10^{-11}$  mbar. The total energy resolution was 6 meV, and the angular resolution was  $0.3^\circ$ . The temperature for the measurements was 9 K. We placed the samples into the sample chamber of the Thermo Scientific K- $\alpha$  XPS instrument and fed the samples into the analysis chamber when the pressure was less than  $2.0 \times 10^{-7}$  mbar. The measured spot size was 400  $\mu\text{m}$ , the operating voltage was 12 kV, and the filament current was 6 mA; the narrow spectrum scanning fluence energy was 50 eV in 0.1 eV steps. Raman spectra were recorded by using an HR-Evolution 2 Raman system at room temperature. A laser with a wavelength of 532 nm and a power of 5.0 mW was used, and the size of the laser spot was about 20  $\mu\text{m}$ .

**2.3. Density Functional Theory Calculations.** The Er adsorption energies, the FD formation energies, and the band structures of the EG in the presence of Er atoms were calculated based on density functional theory (DFT) with the projector-augmented-wave (PAW) method<sup>23</sup> as implemented in the Vienna Ab initio Simulation Package (VASP).<sup>24,25</sup> The Perdew–Burke–Ernzerh of generalized gradient approximation<sup>26</sup> was employed for the electron exchange–correlation functional. A plane-wave cutoff energy of 500 eV was used in all of the calculations. An out-of-plane vacuum space was set to

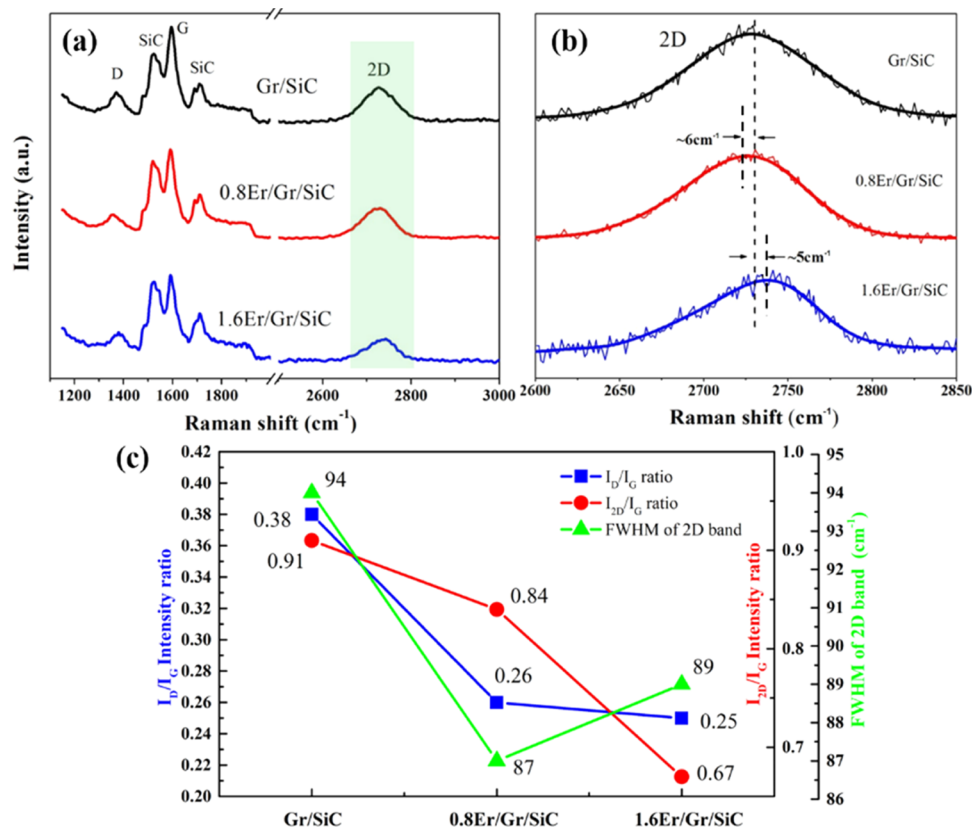


**Figure 2.** (a) Raman spectra of EGs, 0.8 and 1.6 ML Er-doped graphene grown on SiC; (b) enlarged part of the 2D band region of (a); and (c) blue square, green triangle, and red circle represent for the intensity ratios of the D band and G band, those of the 2D band and G band, and the fwhm's of the 2D band, respectively.

>20 Å to eliminate the interlayer interactions. The Er adsorption energy  $E_{\text{ads}}$  is defined as  $E_{\text{ads}} = E_{\text{Er}/\text{substrate}} - E_{\text{substrate}} - E_{\text{Er}}$ , where  $E_{\text{Er}/\text{substrate}}$  is the total energy of the carbon substrate (graphene or FD) with the Er adatoms attached,  $E_{\text{substrate}}$  is the total energy of the pristine graphene or the FD layer, and  $E_{\text{Er}}$  is the total energy of an isolated Er atom. For the calculations of Er adsorption energies, a  $4 \times 4$  supercell was used. The structural parameters and ionic positions were fully optimized until the residual force on each atom was less than 0.01 eV/Å. The first Brillouin zone (BZ) was sampled with  $k$  meshes of  $9 \times 9 \times 1$  by using the  $\gamma$ -centered Monkhorst–Pack method. The convergence threshold for the total energies was set to  $10^{-5}$  eV. To calculate the FD formation energy, a  $9 \times 9 \times 1$  supercell with 162 atoms was used to simulate the graphene with a flower defect. In this case, the force convergence criterion was set to 0.05 eV/Å to reduce the computational expense. The first BZ was sampled with  $k$  meshes of  $3 \times 3 \times 1$  for this large supercell model. Because the correlation effect is important in determining the electronic and magnetic properties of 4f electrons, the Hubbard  $U$  interaction was considered in the calculations with the parameters  $U$  and  $J$  of 6.50 and 0.70 eV, respectively.<sup>27</sup> No SiC substrate was included in the DFT calculations since our investigation has sought to highlight the intrinsic role played by Er atoms.

### 3. RESULTS AND DISCUSSION

Figure 1(a) displays a 500 nm  $\times$  500 nm typical STM image of the pristine EG/SiC surface in which several steps can be distinguished according to the color contrast. The sample

surface is often observably rough, dotted with some clusters, and its steps appear to be broken. When the SiC substrate with erbium atoms predeposited is annealed through the same temperature treatments, the morphology of the EG/SiC surface will be quite different.<sup>28</sup> The morphological evolution of the sample surface as a function of Er coverage is shown in Figure 1(b,c), along with that of ErSi<sub>2</sub> nanostructures. In Figure 1(b), the sample with 0.8 ML Er grown displays clean and smooth surface terraces, which are closely related to Er growth on the SiC substrate.<sup>28</sup> It is also observed that many ErSi<sub>2</sub> nanoislands are pinned at the forefront of upper terraces after annealing, leading to a zigzag edge formation. These nanoislands are roughly uniform in size, ranging from 6 to 24 nm, and occupy ~2.9% of the entire surface area. If the deposition duration of Er flux is elongated (such as 1.6 ML Er), the areal concentration of nanoislands will be increased (~40.3%). When 1.6 ML Er is deposited, the morphology of samples after annealing shows obvious difference. As shown in Figure 1(c), ErSi<sub>2</sub> nanoislands are significantly larger and more irregularly shaped. Some large nanoislands on the EG even have a multilayered structure (see Figure S1). Steps disappear on the sample surface, and the previously separate adjacent terraces have grown into a whole one, greatly enlarging the area.

In the LEED pattern of Figure 1(f), SiC(S) and graphene-(G) spots are marked, and the surrounding hexagon “6  $\times$  6” spots are sharper in contrast to those in Figure 1(d), which indicates that the graphitization degree of the sample in Figure 1(c) is higher. STM and LEED results manifest that Er deposition can confine the sublimation of Si atoms and

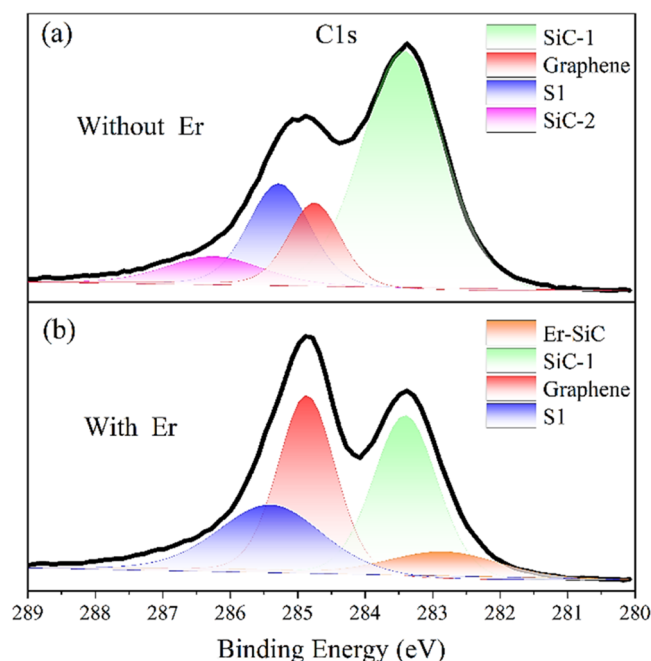
decrease the activation energy for C atoms to diffuse so as to promote the growth of large graphene domains, just like thermal decomposition of SiC in an Ar atmosphere,<sup>28,29</sup> and the sample graphitization improves with increasing Er coverage. As the terrace size becomes larger, ridge-like features are also observed on EG in the STM image (as marked in Figure 1(c)). They are in fact bulged regions of the graphene layer, occurring as a result of bending and buckling to relieve the compressive strain.<sup>30</sup> These results are of great significance for the preparation of a large-area functional EG.

Figure 2(a) displays the Raman spectra of EG with different Er coverages on SiC upon thermal decomposition, and the Raman spectrum obtained on pristine EG is presented for comparison. The Raman spectrum of EG shows the defect-induced D band, pointing to the existing defects which result from the corrugation, surface doping, or the interaction of graphene with vacancies and substrate. The intensity ratio of D/G bands ( $I_D/I_G$ ) is always utilized to estimate the quantity of defects in graphene.<sup>31</sup> As displayed by the blue squares in Figure 2(c), the value of  $I_D/I_G$  decreases from 0.38 to 0.25 with elevating Er coverage gradually, indicating that the defects in the graphene layer become smaller in amount. Overall, Er atoms play an important role in the growth mode and fabrication quality of epitaxial graphene, consistent with our previous investigations.<sup>28</sup>

It is known that the 2D peak is related to the intervalley double resonant Raman scattering.<sup>32</sup> The full width at half maximum (fwhm) of the 2D peak is often used to determine the number of graphene layers. For further analysis, the 2D bands in Figure 2(a) are displayed more clearly in the enlarged graph plotted in Figure 2(b). The fwhm of the 2D peak obtained on the pristine graphene is found to be  $94\text{ cm}^{-1}$ , while those on the 0.8 and 1.6 ML Er-deposited graphene are  $87$  and  $89\text{ cm}^{-1}$ , respectively. These values lie between those for the monolayer and bilayer graphene ( $60\text{--}95\text{ cm}^{-1}$ ),<sup>33</sup> attributed to the coexistence of the monolayer and bilayer graphene on the samples. This result indicates that Er predeposition can inhibit the growth of multilayer graphene to a certain extent, and the lower 2D band also reveals the reduction in the growth rate of EG on SiC. As the Er coverage increases, the 2D peaks, perceived sensitive to electron/hole doping and strain effects,<sup>34</sup> show a small change in position as exhibited in Figure 2(b). The 0.8 ML Er-predeposited graphene is found to be predominantly electron-doped, with an increase in electron concentration leading to a  $6\text{ cm}^{-1}$  red shift in the 2D peak. For the 1.6 ML Er-predeposited graphene, the 2D peak shows a  $5\text{ cm}^{-1}$  blue shift, which is considered to originate from the strain effect.<sup>35</sup> With the Er coverage increasing, the volume and density of  $\text{ErSi}_2$  nanoislands increase; they are believed to cause the compressive strain on EG and enhance the interaction of the SiC substrate with EG, whereby the strain changes the lattice constant of graphene and hence the 2D peak positions. In the case of 1.6 ML Er, the strain effect is more dominant than the doping effect, corresponding with the experimental observation of ridge formation in Figure 1(c). In addition, the intensity ratio of the 2D and G peaks is related to the doping concentration of graphene.<sup>34</sup> With Er coverage increasing, the decrease of  $I_{2D}/I_G$  (from 0.91 to 0.67) means that the doping concentration increases.

In order to gain insights into the influence of Er predeposition and the chemical bonding environments of the samples, the C 1s core-level measurements have been carried

out for pristine and 1.6 ML Er-predeposited graphene with a photon energy of  $1486.6\text{ eV}$ . As shown in Figure 3(a), the C 1s



**Figure 3.** XPS C 1s spectra of samples (a) without Er and (b) with 1.6 ML Er after annealing at  $1300\text{ }^\circ\text{C}$ . Black solid curves are the experimental data, and the color curves are the envelope lines of the fitted components.

photoelectron spectrum for the pristine graphene can be decomposed into four distinctive components. The peaks at binding energies of  $283.4\text{ eV}$  (SiC-1) and  $286.3\text{ eV}$  (SiC-2) stem from the SiC substrate<sup>36,37</sup> with the graphene component at  $284.7\text{ eV}$ . The remaining component S1 is related to the buffer layer, due to C atoms in the  $6\sqrt{3}$  buffer layer bonding to one topmost Si atom of the SiC substrate and to three C atoms of the same  $\text{sp}^2$ -bonded layer.<sup>38,39</sup> After Er deposition (Figure 3(b)), no visible changes can be found in the binding energy locations of three components (SiC-1, graphene, and S1) with respect to the pristine graphene. The disappearance of the previous SiC-2 component and the weakening of the SiC-1 component may be due to the  $\text{ErSi}_2$  islands covering the sample surface, resulting in the XPS signal from the part of the SiC substrate to be undetectable. The additional component located at  $282.8\text{ eV}$  (labeled as “Er-SiC”) can be explained by the fact that the C 1s spectrum contains contributions from both the unperturbed and Er-deposited graphene regions. This new component which appears at  $282.8\text{ eV}$  is ascribed to the contribution of the C atoms in the SiC substrate located just beneath the  $\text{ErSi}_2$  layer and is shifted by  $\sim 0.6\text{ eV}$  from the bulk SiC component to lower binding energy. Similar shifted components of the C 1s signal have already been reported for some intercalated systems, such as H-, Si-, and Li-intercalated graphene.<sup>40–43</sup> This shift can be reasonably linked to the surface band bending induced by the intercalation of a small amount of Er atoms, and it also implies the charge modification at the interface region with the formation of Er–Si bonds.<sup>44</sup>

Our previous study has confirmed that Er predeposition can modify the category of structural defects in graphene.<sup>28</sup> As shown in Figure 4(a), there are appreciable amounts of defects

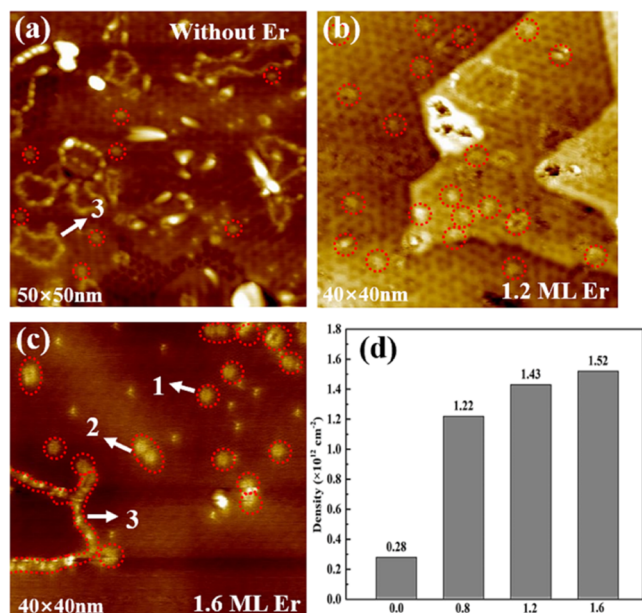


**Figure 4.** STM images of (a) pristine graphene and (b) 1.2 ML and (c) 1.6 ML Er-deposited graphene after annealing at 1300 °C. (d) Histogram of the density of flower defects in graphene at different Er coverages. Tunneling conditions: (a)  $-1.2$  V,  $0.6$  nA; (b)  $-1.5$  V,  $0.7$  nA; and (c)  $-0.8$  V,  $0.6$  nA.

probed on the pristine graphene surface as a result of the rapid sublimation of Si atoms and the fast reconfiguration of C atoms. The flower defect (FD), the smallest grain boundary loop encompassing 24 central atoms, is composed of six pentagon–heptagon rings arranged with  $C_6$  symmetry.<sup>45</sup> Er atoms grown on SiC may generate high-density FDs in EG, but the coverage dependence of the FD and the formation mechanism induced by Er are still unclear. We need, therefore, to conduct in-depth research. Based on the results of 0.8 ML Er predeposition in ref 28., the Er coverage has been further increased to 1.2 and 1.6 ML. The FD distributions on the annealed sample surfaces are shown in Figure 4(b,c). The FD marked by arrow 1 in Figure 4(c) is by far prevailing, which has the lowest formation energy per pentagon–heptagon pair among the rotational grain boundaries and is almost fully strain relaxed.<sup>45</sup> A few conjoined twin defects have also been observed and are marked by arrow 2. In addition, single or incomplete FDs often merge with adjacent FDs and form ring structure defects as marked by arrow 3, to lower their perturbation to the lattice.<sup>46</sup> It is also noticed that the density of FDs increases from  $0.28 \times 10^{12}$  to  $1.52 \times 10^{12}$   $\text{cm}^{-2}$  for 1.6 ML Er growth, approximately 5 times as much as that of the pristine graphene. We took 10 different areas of each sample for STM measurements and averaged the obtained flower defect densities. The statistical results are plotted into a histogram in Figure 4(f); it is shown that the areal density of FDs increases with the rising Er coverage and this trend is particularly evident in the cases where Er coverage is relatively low. STM results show that FD positions are random. It is known that electronic properties of bilayer graphene may depend on the positions of FDs relative to the underlying graphene, and FDs belonging to the same domain are more or less in interaction with others in vicinity and this interaction could induce inhomogeneous stress, which is of great importance to the local mechanical properties.<sup>47</sup>

FDs have a wide range of potential applications in nanoelectronics, such as (1) inducing considerable modifications of transport properties compared to other point-like defects;<sup>48</sup> (2) separating electrons from holes and filtering electrons in a certain energy range;<sup>49</sup> (3) creating a high spin polarization in zigzag graphene nanoribbons;<sup>50</sup> and (4) opening a band gap for graphene.<sup>51</sup> Therefore, the generation of FDs with high density is of great significance for tuning graphene electronic properties. Till now, the approach on how to prepare high-density FDs in graphene is very rare, especially on the Si-rich SiC(0001) substrate. In relation to Au atoms used as an activator to control synthesis of graphene with high-density FDs on the C-terminated SiC(0001) surface,<sup>52</sup> our Er predeposition method is simple and economical, with a one-step fabrication process that does not contain multiple metal depositions and thermal treatments. It provides a new and effective route to control high-density FD formation in EG on the SiC Si-rich surface.

We theoretically investigate the role of Er atoms in FD formation by using first-principles calculations. The Er adsorption energies ( $E_{\text{ads}}$ ) for Er atoms on graphene and FDs are calculated first (see Section 2.3), which can give the most stable adsorption sites for Er atoms on graphene or FDs. As shown in Figure 5(a–c), three typical adsorption sites

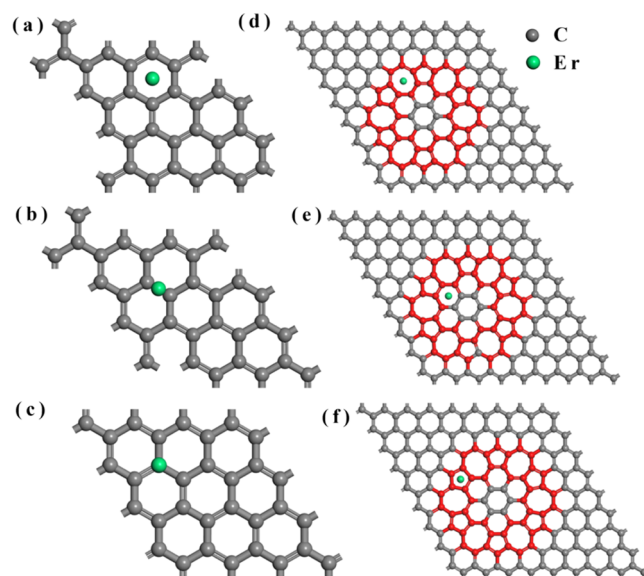


**Figure 5.** Structural diagrams of Er atoms at different adsorption sites in pristine graphene (a–c) and graphene with FDs (d–f).

(hollow, bridge, and top) are considered for the Er atoms on the pristine graphene. The calculated adsorption energies are given in Table 1. The more negative the  $E_{\text{ads}}$  is, the stronger the Er atom adheres to the carbon substrate. Thus, for Er atoms on pristine graphene, the most stable adsorption

**Table 1.**  $E_{\text{ads}}$  of the Er Atom at Each Adsorption Site<sup>a</sup>

	adsorption sites		
graphene	<b>hollow</b>	bridge	top
$E_{\text{ads}}$ (eV)	<b>-1.51</b>	-1.41	-1.42
FD	<b>heptagonal hollow</b>	hexagonal hollow	pentagonal hollow
$E_{\text{ads}}$ (eV)	<b>-3.00</b>	-2.60	-2.63

<sup>a</sup>The most stable adsorption sites are shown in bold.

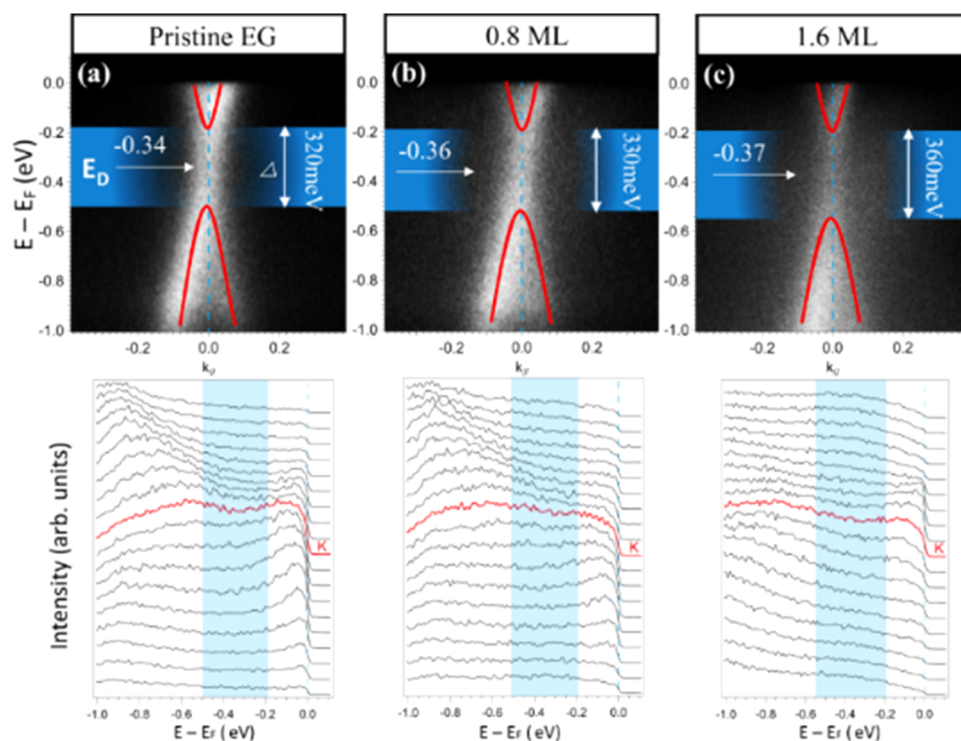


**Figure 6.** Dispersion of the  $\pi$  bands measured with ARPES along the  $\Gamma$ – $K$ – $M$  direction of the graphene Brillouin zone for EG on the SiC(0001) surface around the  $K$ -point of (a) pristine EG and Er-doped EG with increasing Er coverage: (b) 0.8 ML and (c) 1.6 ML.

position is the hollow site. Based on this, three hollow adsorption sites, heptagonal hollow, hexagonal hollow, and pentagonal hollow, are considered for Er on FD (Figure 5(d–f)). Clearly, the most stable adsorption site for one Er atom on the FD is at the center of one of the heptagonal rings of the FD (Table 1).

The FD formation energy  $E_f^{52}$  in the presence of Er atoms is calculated through  $E_f = E(\text{FD} + \text{Er}) - E(\text{GR} + \text{Er})$ , where the first right-hand side term is the total energy of the FD in graphene with one Er atom adsorbed and the second one is the total energy of the corresponding pristine graphene structure also with one Er atom. The  $E_f$  without Er atoms is first calculated, giving the value of 7.20 eV, in agreement with previous results.<sup>45,52</sup> The  $E_f$  becomes 5.79 eV when one Er atom is adsorbed, indicating a significant decrease of the formation energy. This trend manifests that Er atoms play a catalytic role in the dramatic increasing of FD in graphene.

It is known that the origin of FDs in graphene remains an open question until now.<sup>28</sup> Our results about Er predeposition may provide some clues to the generation mechanism of FDs during graphene growth. The following two facts should be given attention: (1) the Raman spectrum shows that the presence of 1.6 ML Er atoms can cause the blue shift of 2D peaks, indicating that the addition of Er atoms changes the surface stress and (2) STM results display that after Er deposition, many ridge structures appear on the sample surface as the Er coverage increases, and the appearance of ridge structures is one of the manifestations for the altered surface stress. Therefore, we believe that the surface stress is a very important cause to result in the FD formation in pristine graphene as well as the significant increase of its areal density in Er-deposited graphene.

According to the results of experimental observations and stress-related analyses, the promoting mechanism of Er to the

increase of FDs in Er-deposited graphene is discussed in the following two main points: (i) Incorporation of new surface components: When Er is deposited on SiC, most Er atoms react with Si atoms to form numerous  $\text{AlB}_2$ -type  $\text{ErSi}_2$  nanoislands, triggered by heating decomposition during the SiC graphitization process. Due to a lattice constant of 0.246 nm for graphene, 0.308 nm for 4H-SiC, and 0.379 nm for  $\text{AlB}_2$ -type  $\text{ErSi}_2$ , large lattice mismatch usually leads to an increase in stress of the sample surface. (ii) Atomic doping: During high-temperature annealing of the Er-deposited SiC, some Er atoms are probably assembled into particles or directly inserted between C atoms, besides growing into  $\text{ErSi}_2$  islands. There exists probability that a few Er atoms doped in the growing graphene layer will undergo sublimation and result in the generation of vacancies and dislocations. Vacancies and dislocations often produce dangling bonds and abnormal structures, more likely to form new defects. This situation is just like Bi atoms bonding with C atoms after introduced in graphene, which bring about the formation of dislocations and other non-six carbon ring defects.<sup>53</sup> Therefore, the existing  $\text{ErSi}_2$  nanoislands and Er particles can induce locally intense stress and its distribution in the graphitizing layer, thereby increasing the elastic energy. In order to relieve stress and relax the graphene lattice, C atom reorganization happens during annealing, five- and seven-carbon rings will be generated locally and are finally composed into FDs. As a result, the density of FDs in the Er-deposited graphene increases much greatly than that in pristine graphene.

Based on the above-mentioned analysis, we preliminarily speculate that the FDs in pristine graphene originate from the surface stress during lattice formation. During the SiC graphitization, high temperature causes Si atoms to sublimate from the surface after SiC thermal decomposition, resulting in local stress in the growing graphitizing lattice. As a result, the

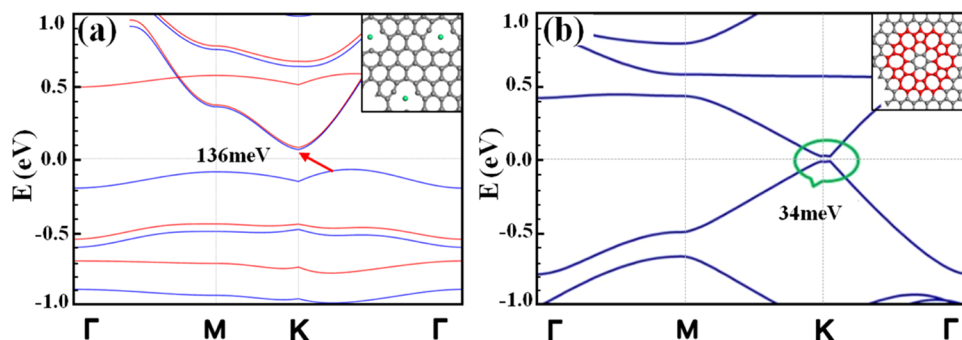


**Figure 7.** Calculated band structures of graphene with (a) Er doping and (b) FD individually. The insets show the corresponding atomic configurations.

atomic structures of the strained regions change and distort, leading to the emergence of five- and seven-carbon ring structures, which eventually evolve into FDs. Due to its dynamic nature, this evolution process is rarely probed directly. FDs can migrate in graphene and coalesce into conjoined twin defects and even ring structure defects during annealing, and the intermediate stages when two FDs meet and merge into a conjoined twin defect have been captured in the STM experiments.<sup>28</sup> The present work provides only a preliminary exploration of the origin of FDs, and further investigations should be required for a deeper insight into its formation mechanism.

In order to characterize the changes in the electronic structure of EG induced by Er predeposition, we present the progressive changes in the  $\pi$ -band of EG on SiC(0001) near the K-point of the first Brillouin zone induced by the Er doping, as shown in Figure 6. A well-defined linear  $\pi$ -band can be seen from pristine EG with a Dirac point energy ( $E_D$ ) located at 0.34 eV below the Fermi level ( $E_F$ ), exhibiting n-doping of graphene due to the electron transfer from the underlying SiC,<sup>54–56</sup> in agreement with our Raman results. The weaker and fuzzier  $\pi$ -band is noticed when Er atoms are adsorbed, as also seen for Li<sup>57</sup> Na<sup>58</sup> and Cs<sup>59</sup> on graphene. With Er coverage increasing, the  $E_D$  of EG gradually shifts away from  $E_F$  (from  $-0.34$  to  $-0.37$  eV). During the thermal decomposition of SiC and the subsequent growth of EG, some Er atoms are synchronously doped into the EG layer. Such local electronic states are characteristic of Er dopants, indicating that the n-doping behavior is enhanced owing to the electron transfer from Er dopants to the EG layer. In addition to the n doping, Er leads to a band gap at  $E_D$ . The gap width  $\Delta E$  is estimated from the distance between the two vertices of the hyperbola. The pristine EG in Figure 6(a) originally has a gap of 320 meV, and the origin of this gap is the breaking of sublattice symmetry owing to the graphene–substrate interaction.<sup>54</sup> As shown in Figure 6(b,c), the band gap of EG is further widened after the introduction of Er atoms and increases gradually with increasing coverage of the atoms (from 320 to 360 meV). This follows from an analysis of the respective energy distribution curves.

To understand the mechanism for this band gap opening, we have performed some investigations by means of first-principles calculations. Since Er atoms are actually involved in the SiC thermal decomposition and the whole graphitization process at high temperature, it is very likely that some C atoms will be replaced by Er atoms during the graphene formation process, resulting in substitution doping. According to the above-mentioned experimental results, Er doping and induced

FDs may be two factors affecting the graphene band structures. We have constructed the structural models for graphene with Er substitution doping (doping concentration of  $\sim 3.12\%$ ) and graphene with a single FD, and we calculated the corresponding band structures. An indirect band gap of 136 meV is opened when Er substitution doping occurs in graphene, as shown in Figure 7(a). This calculation result is sufficient to demonstrate the contribution of Er doping to the band gap opening in EG. Based on previous studies,<sup>60–62</sup> it is reasonably speculated that the band gap opening induced by Er doping may also stem from the following justification: because of strong covalent orbital hybridization and charge redistribution, Er atoms adsorbed on or intercalated under the graphene layer act as dopants to tailor and functionalize graphene, which enhances the interaction between EG and the SiC substrate; external perturbation introduced through Er predeposition further breaks the sublattice symmetry between the two equivalent carbon sublattices of graphene. We also use 198 C atoms to form a graphene lattice containing a single FD. The band structure of graphene calculated by means of DFT theory is shown in Figure 7(b), where a 34 meV energy gap is opened in graphene due to the appearance of FDs. Therefore, our experiments and DFT calculations reveal that the band gap of EG can be tuned by the cooperative action of Er doping and high-density FDs. Due to the FD density used in the DFT calculations being about 1 order of magnitude larger than that of the actual FD density in the Er-deposited graphene, it is manifested that Er doping is more important for band gap opening in graphene. The finding will be helpful in the modification of electronic properties of EG-based devices.

#### 4. CONCLUSIONS

In conclusion, the effects of Er predeposition on flower defects and electronic properties of epitaxial graphene on SiC(0001) have been investigated by using STM observations, spectroscopy measurements, and DFT calculations. Experimental results show that Er atoms have a catalytic effect on flower defects in EG and that the areal density of FDs increases with Er coverage rising. First-principles calculations provide direct evidence for a drastic decrease in the FD formation energy after Er deposition. It is believed that the promoting effect of Er atoms on FD formation is due to the stress in the graphitizing carbon lattice induced by Er doping and its silicide nanoislands. Er predeposition can also modify the electronic doping and surface charge properties of EG, and lowering of the Dirac point energy away from the Fermi level is observed, indicating an enhancement of n-doping in EG. Of particular importance is that Er atoms can open a band gap in EG

broadening with increasing Er coverage, which is brought about by the cooperative action of Er doping and high-density flower defects. This scheme of introducing and tuning a band gap in EG may be helpful to apply EG to future graphene-based nanoelectronics.

## ■ ASSOCIATED CONTENT

### SI Supporting Information

The Supporting Information is available free of charge at <https://pubs.acs.org/doi/10.1021/acsomega.3c06523>.

STM images of large nanoislands with a multilayered structure on the EG (PDF)

## ■ AUTHOR INFORMATION

### Corresponding Author

Qun Cai – State Key Laboratory of Surface Physics and Department of Physics, Fudan University, Shanghai 200433, People's Republic of China; [orcid.org/0000-0002-8457-6976](https://orcid.org/0000-0002-8457-6976); Email: [qcai@fudan.edu.cn](mailto:qcai@fudan.edu.cn)

### Authors

Yong Duan – State Key Laboratory of Surface Physics and Department of Physics, Fudan University, Shanghai 200433, People's Republic of China; [orcid.org/0000-0002-7063-1743](https://orcid.org/0000-0002-7063-1743)

Wenting Xu – State Key Laboratory of Surface Physics and Department of Physics, Fudan University, Shanghai 200433, People's Republic of China

Wenxia Kong – State Key Laboratory of Surface Physics and Department of Physics, Fudan University, Shanghai 200433, People's Republic of China

Jianxin Wang – State Key Laboratory of Surface Physics and Department of Physics, Fudan University, Shanghai 200433, People's Republic of China

Jinze Zhang – State Key Laboratory of Surface Physics and Department of Physics, Fudan University, Shanghai 200433, People's Republic of China

Zhongqin Yang – State Key Laboratory of Surface Physics and Department of Physics, Fudan University, Shanghai 200433, People's Republic of China; [orcid.org/0000-0002-4949-1555](https://orcid.org/0000-0002-4949-1555)

Complete contact information is available at: <https://pubs.acs.org/doi/10.1021/acsomega.3c06523>

### Author Contributions

Y.D.: experiment investigation, formal analysis, validation, and writing—original draft, review, and editing. W.X.: DFT calculation, formal analysis, validation, and writing—review and editing. W.K.: experiment investigation, formal analysis, validation, and writing—review and editing. J.W.: experimental investigation, validation, and writing—review and editing. J.Z.: experimental investigation, validation, and writing—review and editing. Z.Y.: supervision, first-principles investigation, formal analysis, and writing—original draft, review, and editing. Q.C.: supervision, experimental investigation, formal analysis, writing—original draft, review, and editing, and project administration.

### Notes

The authors declare no competing financial interest.

## ■ ACKNOWLEDGMENTS

The authors would like to acknowledge the experimental assistance for LEED and ARPES observations from Dr. Y.H.Song and Professor R.Peng, Department of Physics, Fudan University. This work was supported by the Natural Science Foundation of Shanghai Science and Technology Committee under Grant Nos. 18ZR1403300 and 21ZR1408200 and the National Natural Science Foundation of China under Grant Nos. 12174059 and 11874117.

## ■ REFERENCES

- (1) Geim, A. K.; Novoselov, K. S. The Rise of Graphene. *Nat. Mater.* **2007**, *6*, 183–191.
- (2) Geim, A. K.; MacDonald, A. H. Graphene: Exploring CarbonFlatland. *Phys. Today* **2007**, *60*, 35–41.
- (3) Novoselov, K. S.; Jiang, Z.; Zhang, Y.; Morozov, S. V.; Stormer, H. L.; Zeitler, U.; Maan, J. C.; Boebinger, G. S.; Kim, P.; Geim, A. K. Room-Temperature Quantum Hall Effect in Graphene. *Science* **2007**, *315*, No. 1379.
- (4) Tombros, N.; Jozsa, C.; Popinciuc, M.; Jonkman, H. T.; Wees, B. J. Electronic Spin Transport and Spin Precession in Single Graphene Layers at Room Temperature. *Nature* **2007**, *448*, 571–574.
- (5) Novoselov, K. S.; Geim, A. K.; Morozov, S. V.; Jiang, D.; Katsnelson, M. I.; Grigorieva, I. V.; Dubonos, S. V.; Firsov, A. A. Two-Dimensional Gas of Massless Dirac Fermions in Graphene. *Nature* **2005**, *438*, 197–200.
- (6) Endoh, N.; Akiyama, S.; Tashima, K.; Suwa, K.; Kamogawa, T.; Kohama, R.; Funakubo, K.; Konishi, S.; Mogi, H.; Kawahara, M.; Kawai, M.; Kubota, Y.; Ohkochi, T.; Kotsugi, M.; Horiba, K.; Kumigashira, H.; Suemitsu, M.; Watanabe, I.; Fukidome, H. High-Quality Few-Layer Graphene on Single-Crystalline SiC thin Film Grown on Affordable Wafer for Device Applications. *Nanomaterials* **2021**, *11*, No. 392.
- (7) Zhang, Y.; Tan, Y. W.; Stormer, H.; Kim, P. Experimental Observation of The Quantum Hall Effect and Berry's Phase in Graphene. *Nature* **2005**, *438*, 201–204.
- (8) Novoselov, K. S.; Geim, A. K.; Morozov, S. V.; Jiang, D.; Zhang, Y.; Dubonos, S. V.; Grigorieva, I. V.; Firsov, A. A. Experimental observation of the quantum Hall effect and Berry's phase in graphene. *Science* **2004**, *306*, 666–669.
- (9) Balog, R.; Jorgensen, B.; Nilsson, L.; Andersen, M.; Rienks, E.; Bianchi, M.; Fanetti, M.; Laegsgaard, E.; Baraldi, A.; Lizzit, S.; Slijivancin, Z.; Besenbacher, F.; Hammer, B.; Pedersen, T. G.; Hofmann, P.; Hornekaer, L. Bandgap opening in graphene induced by patterned hydrogen adsorption. *Nat. Mater.* **2010**, *9*, 315–319.
- (10) Norimatsu, W.; Kusunoki, M. Epitaxial graphene on SiC(0001): advances and perspectives. *Phys. Chem. Chem. Phys.* **2014**, *16*, 3501–3511.
- (11) Kruskopf, M.; Pakdehi, D. M.; Pierz, K.; Wundrack, S.; Stosch, R.; Dziomba, T.; Götz, M.; Baringhaus, J.; Aprojanz, J.; Tegenkamp, C.; Lidzba, J.; Seyller, T.; Hohls, F.; Ahlers, F. J.; Schumacher, H. W. Comeback of epitaxial graphene for electronics: large-area growth of bilayer-free graphene on SiC. *2D Mater.* **2016**, *3*, No. 041002.
- (12) Walter, A. L.; Nie, S.; Bostwick, A.; Kim, K. S.; Moreschini, L.; Chang, Y. J.; Innocenti, D.; Horn, K.; McCarty, K. F.; Rotenberg, E. Electronic structure of graphene on single-crystal copper substrates. *Phys. Rev. B* **2011**, *84*, No. 195443.
- (13) Castro, E. V.; Novoselov, K. S.; Morozov, S. V.; Peres, N. M. R.; dos Santos, J. M. B. L.; Nilsson, J.; Guinea, F.; Geim, A. K.; Neto, A. H. C. Biased Bilayer Graphene: Semiconductor with a Gap Tunable by the Electric Field Effect. *Phys. Rev. Lett.* **2007**, *99*, No. 216802.
- (14) Son, Y. W.; Cohen, M. L.; Louie, S. G. Energy Gaps in Graphene Nanoribbons. *Phys. Rev. Lett.* **2006**, *97*, No. 216803.
- (15) Wang, C.; Wang, H.; Chen, W.; Xie, X. Direct observation of global elastic intervalley scattering induced by impurities on graphene. *Nano Lett.* **2021**, *21*, 8258–8265.

- (16) Hu, T.; Yang, D.; Hu, W.; Xia, Q.; Ma, F.; Xu, K. The structure and mechanism of large-scale indium-intercalated graphene transferred from SiC buffer layer. *Carbon* **2021**, *171*, 829–836.
- (17) Warmuth, J.; Bruix, A.; Michiardi, M.; Hånke, T.; Bianchi, M.; Wiebe, J.; Wiesendanger, R.; Hammer, B.; Hofmann, P.; Khajetoorians, A. A. Band-gap engineering by Bi intercalation of graphene on Ir(111). *Phys. Rev. B* **2016**, *93*, No. 165437.
- (18) Gao, T.; Gao, Y.; Chang, C.; Chen, Y.; Liu, M.; Xie, S.; He, K.; Ma, X.; Zhang, Y.; Liu, Z. Atomic-scale morphology and electronic structure of manganese atomic layers underneath epitaxial graphene on SiC(0001). *ACS Nano* **2012**, *6*, 6562–6568.
- (19) Guo, H.; Zhang, R.; Li, H.; Wang, X.; Lu, H.; et al. Sizable Band Gap in Epitaxial Bilayer Graphene Induced by Silicene Intercalation. *Nano Lett.* **2020**, *20*, 2674–2680.
- (20) Sandin, A.; Jayasekera, T.; Rowe, J. E.; Kim, K. W.; Nardelli, M. B.; Dougherty, D. B. Multiple coexisting intercalation structures of sodium in epitaxial graphene-SiC interfaces. *Phys. Rev. B* **2012**, *85*, No. 125410.
- (21) Anderson, N. A.; Hupalo, M.; Keavney, D.; Tringides, M.; Vaknin, D. Intercalated rare-earth metals under graphene on SiC. *J. Magn. Magn. Mater.* **2019**, *474*, 666–670.
- (22) Chen, G.; Wan, J.; Yang, J.; Ding, X.; Ye, L.; Wang, X. Surface structures of erbium silicide ultra-thin films formed by solid phase epitaxy on Si(100). *Surf. Sci.* **2002**, *513*, 203–210.
- (23) Blöchl, P. E. Projector augmented-wave method. *Phys. Rev. B* **1994**, *50*, No. 17953.
- (24) Kresse, G.; Furthmüller, J. Efficiency of ab-initio total energy calculations for metals and semiconductors using a plane-wave basis set. *Comput. Mater. Sci.* **1996**, *6*, 15–50.
- (25) Kresse, G.; Furthmüller, J. Efficient iterative schemes for ab initio total-energy calculations using a plane-wave basis set. *Phys. Rev. B* **1996**, *54*, 11169–11186.
- (26) Perdew, J. P.; Chevary, J. A.; Vosko, S. H.; Jackson, K. A.; Pederson, M. R.; Singh, D. J.; Fiolhais, C. Atoms, molecules, solids, and surfaces-applications of the generalized gradient approximation for exchange and correlation. *Phys. Rev. B* **1992**, *46*, 6671–6687.
- (27) Huang, Z.; Ye, L.; Yang, Z. Q.; Xie, X. Interaction between Er atoms and the carbon cage C<sub>82</sub>. *Phys. Rev. B* **2000**, *61*, 12786–12791.
- (28) Duan, Y.; Kong, W.; Zhang, J.; Wang, J.; Cai, Q. Effects of Er atoms on graphitization process and structural defects for epitaxial graphene. *J. Appl. Phys.* **2022**, *132*, No. 135701.
- (29) Emtsev, K. V.; Bostwick, A.; Horn, K.; Jobst, J.; Kellogg, G. L.; Ley, L.; McChesney, J. L.; Ohta, T.; Reshanov, S. A.; Röhrl, J.; Rotenberg, E.; Schmid, A. K.; Waldmann, D.; Weber, H. B.; Seyller, T. Towards wafer-size graphene layers by atmospheric pressure graphitization of silicon carbide. *Nat. Mater.* **2009**, *8* (3), 203–207.
- (30) Sun, G. F.; Jia, J. F.; Xue, Q. K.; Li, L. Atomic-scale imaging and manipulation of ridges on epitaxial graphene on 6H-SiC(0001). *Nanotechnology* **2009**, *20* (35), No. 355701.
- (31) Ferrari, A. C.; Basko, D. M. Raman spectroscopy as a versatile tool for studying the properties of graphene. *Nat. Nanotechnol.* **2013**, *8* (4), 235–246.
- (32) Chan, S. H.; Chen, S. H.; Lin, W. T.; Li, M. C.; Lin, Y. C.; Kuo, C. C. Low-temperature synthesis of graphene on Cu using plasma-assisted thermal chemical vapor deposition. *Nanoscale Res. Lett.* **2013**, *8* (1), No. 285.
- (33) Ni, Z. H.; Chen, W.; Fan, X. F.; Kuo, J. L.; Yu, T.; Wee, A. T. S.; Shen, Z. X. Raman Spectroscopy of Epitaxial Graphene on a SiC Substrate. *Phys. Rev. B* **2008**, *77* (11), No. 115416.
- (34) Casiraghi, C.; Pisana, S.; Novoselov, K. S.; Geim, A. K.; Ferrari, A. C. Raman fingerprint of charged impurities in graphene. *Appl. Phys. Lett.* **2007**, *91* (23), No. 233108.
- (35) Röhrl, J.; Hundhausen, M.; Emtsev, K. V.; Seyller, T.; Graupner, R.; Ley, L. Raman spectra of epitaxial graphene on SiC(0001). *Appl. Phys. Lett.* **2008**, *92* (20), No. 201918.
- (36) Jernigan, G. G.; VanMil, B. L.; Tedesco, J. L.; Tischler, J. G.; Glaser, E. R.; Davidson, A.; Campbell, P. M.; Gaskill, D. K. Comparison of Epitaxial Graphene on Si-face and C-face 4H SiC Formed by Ultrahigh Vacuum and RF Furnace Production. *Nano Lett.* **2009**, *9*, 2605–2609.
- (37) Hu, T. W.; Liu, X. T.; Ma, F.; Ma, D. Y.; Xu, K. W.; Chu, P. K. High-quality, single-layered epitaxial graphene fabricated on 6H-SiC(0001) by flash annealing in Pb atmosphere and mechanism. *Nanotechnology* **2015**, *26*, No. 105708.
- (38) Emtsev, K. V.; Speck, F.; Seyller, T.; Ley, L.; Riley, J. D. Interaction, growth, and ordering of epitaxial graphene on SiC{0001} surfaces: A comparative photoelectron spectroscopy study. *Phys. Rev. B* **2008**, *77*, No. 155303.
- (39) Yu, C.; Chen, X.; Zhang, F.; Sun, L.; Li, T.; Xu, X.; Zhao, X. Uniform coverage of quasi-free standing monolayer graphene on SiC by hydrogen intercalation. *J. Mater. Sci.: Mater. Electron.* **2017**, *28*, 3884–3890.
- (40) Riedl, C.; Coletti, C.; Iwasaki, T.; Zakharov, A. A.; Starke, U. Quasi-Free-Standing Epitaxial Graphene on SiC Obtained by Hydrogen Intercalation. *Phys. Rev. Lett.* **2009**, *103*, No. 246804.
- (41) Virojanadara, C.; Watcharinyanon, S.; Zakharov, A. A.; Johansson, L. I. Epitaxial graphene on 6H-SiC and Li intercalation. *Phys. Rev. B* **2010**, *82*, No. 205402.
- (42) Bisti, F.; Profeta, G.; Vita, H.; Donarelli, M.; Perrozzini, F.; Sheverdyaeva, P. M.; Moras, P.; Horn, K.; Ottaviano, L. Electronic and geometric structure of graphene/SiC(0001) decoupled by lithium intercalation. *Phys. Rev. B* **2015**, *91*, No. 245411.
- (43) Xia, C.; Watcharinyanon, S.; Zakharov, A. A.; Yakimova, R.; Hultman, L.; Johansson, L. I.; Virojanadara, C. Si intercalation/deintercalation of graphene on 6H-SiC(0001). *Phys. Rev. B* **2012**, *85*, No. 045418.
- (44) Mammadov, S.; Ristein, J.; Koch, R. J.; Ostler, M.; Raidel, C.; Wanke, M.; Vasiliauskas, R.; Yakimova, R.; Seyller, T. Polarization doping of graphene on silicon carbide. *2D Mater.* **2014**, *1*, No. 035003.
- (45) Cockayne, E.; Rutter, G. M.; Guisinger, N. P.; Crain, J. N.; First, P. N.; Stroscio, J. A. Grain boundary loops in graphene. *Phys. Rev. B* **2011**, *83* (19), No. 195425.
- (46) Guisinger, N. P.; Rutter, G. M.; Crain, J. N.; Heiliger, C.; First, P. N.; Stroscio, J. A. Atomic-scale investigation of graphene formation on 6H-SiC(0001). *J. Vac. Sci. Technol., A* **2008**, *26*, 932–937.
- (47) Zhang, J.; Zhao, J. Mechanical properties of bilayer graphene with twist and grain boundaries. *J. Appl. Phys.* **2013**, *113* (4), No. 043514.
- (48) Linhart, L.; Burgdörfer, J.; Libisch, F. Accurate modeling of defects in graphene transport calculations. *Phys. Rev. B* **2018**, *97* (3), No. 035430.
- (49) Cresti, A.; Carrete, J.; Okuno, H.; Wang, T.; Madsen, G. K. H.; Mingo, N.; Pochet, P. Growth, charge and thermal transport of flowered graphene. *Carbon* **2020**, *161*, 259–268.
- (50) Kang, D.; Zhang, C.; Li, H. Spin transport in zigzag graphene nanoribbon with a flower defect. *J. Supercond. Novel Magn.* **2019**, *32* (12), 3927–3931.
- (51) Cui, Y.; Zhang, H.; Chen, W.; Yang, Z.; Cai, Q. Structural evolution of flower defects and effects on the electronic structures of epitaxial graphene. *J. Phys. Chem. C* **2017**, *121* (28), 15282–15287.
- (52) Berrahal, Q.; Chacon, C.; Amara, H.; Bellec, A.; Latil, S.; Repain, V.; Rousset, S.; Lagoute, J.; Girard, Y. High density synthesis of topological point defects in graphene on 6H-SiC (0001). *Carbon* **2020**, *170*, 174–181.
- (53) Hu, T.; Ma, D.; Fang, Q.; Zhang, P.; Liu, X.; Wei, R.; Pan, Y.; Xu, K.; Ma, F. Bismuth mediated defect engineering of epitaxial graphene on SiC(0001). *Carbon* **2019**, *146*, 313–319.
- (54) Zhou, S. Y.; Gweon, G. H.; Fedorov, A. V.; First, P. N.; De Heer, W. A.; Lee, D. H.; Guinea, F.; Castro Neto, A. H.; Lanzara, A. Substrate-induced band gap opening in epitaxial graphene. *Nat. Mater.* **2007**, *6*, 770–775.
- (55) Starke, U.; Riedl, C. Epitaxial graphene on SiC(0001) and SiC(0001̄): from surface reconstructions to carbon electronics. *J. Phys.: Condens. Matter* **2009**, *21*, No. 134016.
- (56) Mallet, P.; Brihuega, I.; Bose, S.; Ugeda, M. M.; Gomez-Rodriguez, J. M.; Kern, K.; Veuillen, J. Y. Role of pseudospin in

quasiparticle interferences in epitaxial graphene probed by high-resolution scanning tunneling microscopy. *Phys. Rev. B* **2012**, *86* (4), No. 045444.

(57) Virojanadara, C.; Watcharinyanon, S.; Zakharov, A. A.; Johansson, L. I. Epitaxial graphene on 6H-SiC and Li intercalation. *Phys. Rev. B* **2010**, *82* (20), No. 205402.

(58) Watcharinyanon, S.; Johansson, L. I.; Xia, C.; Virojanadara, C. Changes in structural and electronic properties of graphene grown on 6H-SiC(0001) induced by Na deposition. *J. Appl. Phys.* **2012**, *111* (8), No. 083711.

(59) Watcharinyanon, S.; Virojanadara, C.; Johansson, L. I. Rb and Cs deposition on epitaxial graphene grown on 6H-SiC(0001). *Surf. Sci.* **2011**, *605* (21–22), 1918–1922.

(60) Elias, D. C.; Nair, R. R.; Mohiuddin, T. M. G.; Morozov, S. V.; Blake, P.; Halsall, M. P.; Ferrari, A. C.; Boukhvalov, D. W.; Katsnelson, M. I.; Geim, A. K.; Novoselov, K. S. Control of Graphene's Properties by Reversible Hydrogenation: Evidence for Graphane. *Science* **2009**, *323*, 610–613.

(61) Jaiswal, M.; Lim, C. H. Y. X.; Bao, Q. L.; Toh, C. T.; Loh, K. P.; Ozyilmaz, B. Controlled Hydrogenation of Graphene Sheets and Nanoribbons. *ACS Nano* **2011**, *5*, 888–896.

(62) Castro Neto, A. H.; Guinea, F.; Peres, N. M. R.; Novoselov, K. S.; Geim, A. K. The electronic properties of graphene. *Rev. Mod. Phys.* **2009**, *81*, No. 109.